Polym. Bull. (2018) 75:2641–2655
https://doi.org/10.1007/s00289-017-2171-3

ORIGINAL PAPER

Crystallization of poly(L-lactide) in the miscible poly(L-lactide)/poly(vinyl acetate) blend induced by carbon nanotubes

Ting Huang[1] · Jing-hui Yang[1] · Nan Zhang[1] · Ji-hong Zhang[1] · Yong Wang[1]

Received: 28 September 2016 / Revised: 18 June 2017 / Accepted: 29 August 2017 /
Published online: 4 September 2017

Abstract In this work, carbon nanotubes (CNTs) were introduced into miscible poly(L-lactide)/poly(vinyl acetate) (PLLA/PVAc) blend and the crystallization behaviors of PLLA with the presence of PVAc and CNTs are systematically discussed. The dispersion state of CNTs was characterized using scanning electron microscope, and the crystallization behaviors of PLLA in different conditions including melt crystallization and cold crystallization were comparatively investigated using polarized optical microscope, differential scanning calorimetry and wide angle X-ray diffraction. The results showed that the crystallization of PLLA was greatly restricted by PVAc. CNTs exhibit apparent nucleation effect, promoting the occurrence of both melt crystallization and cold crystallization. However, the nucleation effect of CNTs in the ternary composites is weakened as compared with that in the binary PLLA/CNTs composites. It was suggested that the relatively higher interfacial affinity between PVAc and CNTs, which possibly resulted in more PVAc molecule rather than PLLA molecule around the surface of CNTs, was the main reason for the reduced nucleation efficiency.

Keywords Poly(L-lactide)/poly(vinyl acetate) · Carbon nanotubes · Crystallization

✉ Jing-hui Yang
yangjinghui_84@163.com

✉ Yong Wang
yongwang1976@163.com

[1] Key Laboratory of Advanced Technologies of Materials (Ministry of Education), School of Materials Science and Engineering, Southwest Jiaotong University, Chengdu 610031, China

Introduction

Poly(L-lactide) (PLLA) has already attracted much attention of researchers in the last decades due to its intriguing characteristics. On the one hand, it exhibits excellent comprehensive mechanical properties (tensile strength and tensile modulus) which are comparable to those of other polyester, such as poly (ethylene terephthalate) (PET) [1]. On the other hand, it can be produced from completely renewable resources ranging from corn, starch, and sucrose. After being used, the PLLA articles can be hydrolyzed completely in the environmental condition, which reduces the negative effect of PLLA waste on the environment. Therefore, PLLA is also called "green plastic" and has been a promising alternative to petroleum-based plastics.

Blending with other polymer is thought to be an efficient way to enlarge the application field of PLLA. So far, different kinds of PLLA-based blends have been developed through blending with other biodegradable polymers such as polyhydroxybutyrate (PHB) [2], poly(ε-caprolactone) (PCL) [3, 4] and poly(ethylene oxide) (PEO) [5], ductile polymers such as polyethylene (PE) [6] and poly(butylene succinate) (PBS) [7], elastomers and/or rubbers [8–13], other polyesters such as PET [14] and polycarbonate (PC) [15] et al. As it is well known, PLLA is a typical semi-crystalline polymer; however, its crystallization ability is relatively weak and usually it exhibits the completely amorphous state through common processing procedures such as extrusion, injection-molding, compression-molding, etc. Although most of the PLLA-based blends are immiscible with poor interfacial interaction, the presence of the second component influences the crystallization behavior of PLLA to a certain degree, attributing to the nucleation-assisting effect from the second component and/or the spherulites growth-accelerating effect [16]. This is very significant since the improved crystallization ability of PLLA endows the PLLA articles with improved promising physical properties.

It has also been reported that PLLA is miscible with several polymers, such as poly (vinyl acetate) (PVAc) [17, 18], poly (methyl methacrylate) (PMMA) [19, 20] and poly (*p*-vinyl phenol) (PVPh) [21]. In these blends, only one glass transition temperature (T_g) is found, indicating the miscibility between the two components in the amorphous region. Due to the strong interaction at the molecular chain level, the crystallization of PLLA in the miscible blends is greatly restricted by the second component, which is also the typical phenomenon about the crystallization of semicrystalline component in the miscible blends in which the amorphous component has a T_g higher than that of the semicrystalline component.

In this work, we attempted to introduce carbon nanotubes (CNTs) into miscible PLLA/PVAc blend to investigate the combined effects of both CNTs and PVAc on crystallization of PLLA. It has been proved previously that CNTs exhibit excellent heterogeneous nucleation effect for the crystallization of PLLA [22–24]. Different from the selective localization of CNTs in an immiscible polymer blend, in which CNTs have a tendency to selective distribute in the phase which exhibits higher affinity to them [25], CNTs possibly exhibit homogeneous distribution in the miscible polymer blends due to the fact that the blends usually exhibit only one

phase in the melt state. Therefore, this work is mainly focused on whether CNTs still exhibit the nucleation effect and promote the crystallization of PLLA phase on one hand; on the other hand, it is expected to know whether CNTs or PVAc mainly determines the crystallization behavior of PLLA in the miscible blends.

Experimental part

Materials

PLLA (2002D) with D-isomer content of 4.3%, M_w of 2.53 × 105 g/mol, melt flow rate (MFR) of 6 g/10 min (190 °C/2.16 kg), and density of 1.24 g/cm^3 was purchased from NatureWorks®, USA. PVAc (LPS-40Ac), M_w of 9.0 × 104 g/mol, was obtained from Ashland Chemical Company, USA. Pristine CNTs were obtained from Chengdu Institute of Organic Chemistry, Chinese Academy of Science (Chengdu, China). The outer and inner diameters of CNTs are 20–30 nm and 5–10 nm, respectively. The length of a single CNT is about 10–50 μm. CNTs were washed and purified with concentrated hydrochloride acid, and the purity is above 95%.

Sample preparation

Modified CNTs were firstly prepared in our laboratory according to the methodology developed in our previous work [26]. After being functionalized by strong acid, some polar groups including carboxyl and hydroxyl were introduced onto the surface of CNTs, which was favorable for the good dispersion of CNTs in the polymer matrix. Prior to melt blending, both PLLA and PVAc were dried in a vacuum oven at 40 °C for 24 h to eliminate the possible effect of moisture. Subsequently, they were melt-compounded with CNTs using an internal mixer at the melt temperature of 190 °C and rotate speed of 60 rpm, and the mixing duration was 8 min. In this work, the weight ratio between PLLA/PVAc was maintained at 80/20 wt/wt, and the content of CNTs was varied from 0.5 to 5 wt%. The sample notation was defined as PLLA/PVAc/CNTs-*x*, where *x* indicated the content (wt%) of CNTs. For example, PLLA/PVAc/CNTs-0.5 indicated that the content of CNTs in the material was 0.5 wt%. And then, the material was compression-molded to prepare the final samples at melt temperature of 190 °C and molding pressure of 5 MPa. Some compression-molded samples were directly characterized, and others were firstly annealed at 80 °C for 30 min and then were further investigated to understand the heterogeneous nucleation effect of CNTs during the cold crystallization process of PLLA.

Scanning electron microscopy (SEM)

The dispersion of CNTs in the composites was characterized using scanning electron microscope (SEM, FEI Inspect, The Netherlands) at an accelerating voltage

of 5.0 kV. The sample was firstly cryogenically fractured in liquid nitrogen and then the fractured surface was sputter-coated with a thin layer of gold.

Polarized optical microscopy (POM)

The isothermal crystallization morphologies of different samples were characterized using polarized optical microscopy (POM, XPN203E, China) with a hot stage. Firstly, a sample of about 5 mg was heated to 190 °C and pressed to obtain a slice with a thickness of about 20 μm. The slice was then maintained at 190 °C for 3 min to erase the thermal and mechanical history. Secondly, the slice was transferred to the hot stage with a setting temperature of 120 °C and maintained at this temperature for 2 h. The crystalline morphologies of samples were taken images using a digital camera.

Differential scanning calorimetry (DSC)

A differential scanning calorimetry (DSC, Netzsch STA 449C Jupiter, Germany) was used to investigate the crystallization and melting behaviors of samples. For the sample as obtained from compression-molding processing, it was firstly heated from 0 to 190 °C at a heating rate of 5 °C/min, maintained at 190 °C for 3 min to erase any thermal history, then the sample was cooled to 0 °C at a cooling rate of 5 °C/min, subsequently, it was heated again to 200 °C at the heating rate of 5 °C/min. The second heating curve was analyzed. For the annealed sample, it was directly heated from 0 to 200 °C at the heating rate of 5 °C/min. The degree of crystallinity (X_{c-DSC}) was calculated according to the following relation:

$$X_{c-DSC} = \frac{\Delta H_m - \Delta H_{cc}}{\Delta H_m^0 \times \phi} \times 100\%, \quad (1)$$

where ΔH_m is the DSC measured value of fusion enthalpy, ΔH_{cc} is the cold crystallization enthalpy obtained during the DSC heating process, ΔH_m^0 is the fusion enthalpy of the completely crystalline PLLA, and ϕ is the weight fraction of PLLA in the sample. Here, the value of ΔH_m^0 of PLLA was selected as 93 J/g [27].

Wide angle X-ray diffraction (WAXD)

The crystalline structures of PLLA in different samples were further investigated using a wide angle X-ray diffraction (WAXD, DX-1000 with Ni-filtered Cu Kα radiation, China). The continuous scanning angle range used in this study was from 5° to 30° at 40 kV and 25 mA. The X_{c-WAXD} was calculated according to the following relation:

$$X_{c-WAXD} = \frac{\sum A_{crystalline}}{\sum A_{crystalline} + \sum A_{amorphous}} \times 100\%, \quad (2)$$

where $A_{crystalline}$ and $A_{amorphous}$ are the fitted areas of the diffraction peaks of crystalline and amorphous, respectively.

Contact angle measurement

The surface tensions of all the components were deduced by the contact angle measurement which was carried out on the surface of compression-molded films of pure PLLA and PVAc. The pellets were compression-molded at 190 °C to obtain films for testing. Contact angle was measured at 20 °C with a drop shape analysis system (KRÜSS, DSA 100). Measurement of a given contact angle was carried out for at least 5 times. Double distilled water (H_2O) and methylene iodide (CH_2I_2) were used as probe liquids.

Results and discussion

Dispersion of CNTs in the composites

Figure 1 shows the morphology of the blank PLLA/PVAc blend and PLLA/PVAc/CNTs composites. As expected, the blank PLLA/PVAc blend shows single-phase morphology feature and it is very difficult to differentiate both PLLA and PVAc from the blend. This is mainly because that the melt was cooled in air condition and the relatively large cooling rate endows the sample with less time to crystallization. Consequently, phase separation induced by crystallization of PLLA is prevented as reported by Li and You [18]. In the PLLA/PVAc/CNTs-1 composite (seen in Fig. 1b), CNTs are homogeneously dispersed in the blend and no CNTs agglomerate can be observed. Furthermore, the presence of CNTs does not induce the phase separation of the composite. Even if the content of CNTs is increased up to 5 wt%, the composite still show the homogeneous distribution of CNTs.

Crystallization and melting behaviors of the composites

The isothermal crystallization behavior of PLLA in different samples was first investigated and the crystallization morphologies are shown in Fig. 2. For making a comparison, the crystallization morphology of pure PLLA is also shown. Pure PLLA exhibits the typical spherulites with average diameter of about 100 μm. In the blank PLLA/PVAc sample, the number of spherulites is reduced and the average diameter of spherulites is also decreased, indicating that both the nucleation density and the spherulites growth rate of PLLA are smaller than those of pure PLLA. This phenomenon can be attributed to the strong interaction at the molecular level between PLLA and PVAc. Since the chain segments of PVAc can not enter into the crystalline cell of PLLA, the presence of PVAc chain segments and the entanglement between PLLA and PVAc hinder the ordering of PLLA chain segments, retarding the nucleation and spherulites growth of PLLA accordingly. However, the addition of a few amounts of CNTs greatly influences the crystallization behavior of PLLA. For example, the sample PLLA/PVAc/CNTs-0.5 exhibits much more spherulites with largely decreased spherulites diameters, apparently different from the sporadic spherulites as observed in the pure PLLA and the blank PLLA/PVAc blend. Increasing the content of CNTs in the composites, the

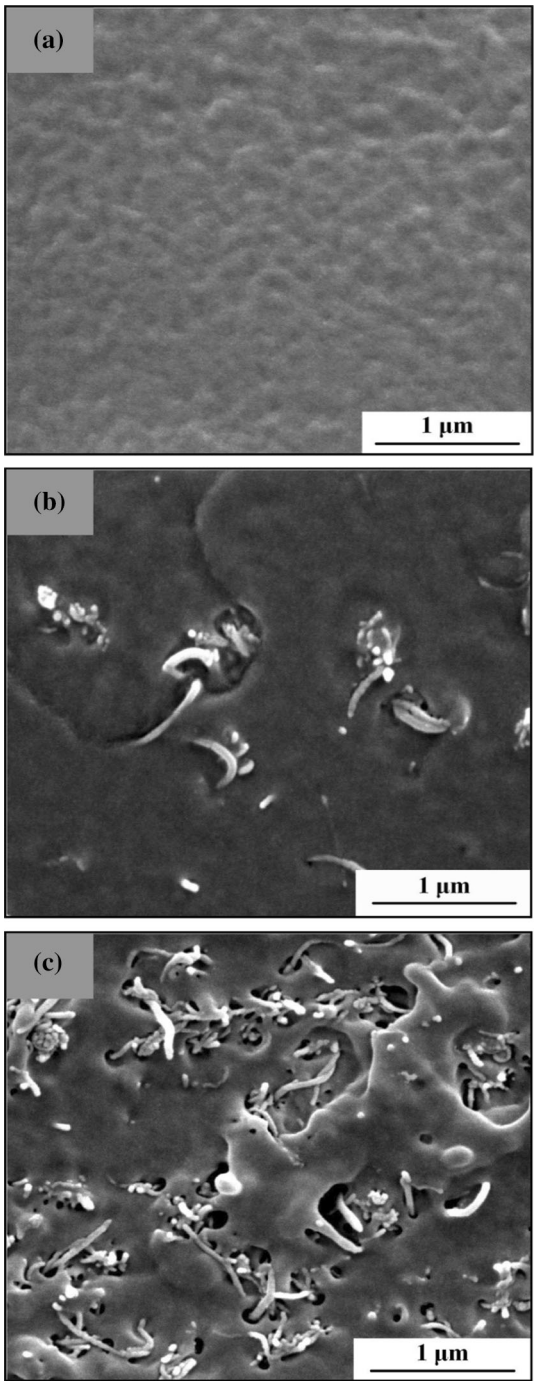

Fig. 1 SEM images showing the morphologies of **a** PLLA/PVAc blend, **b** PLLA/PVAc/CNTs-1 and **c** PLLA/PVAc/CNTs-5

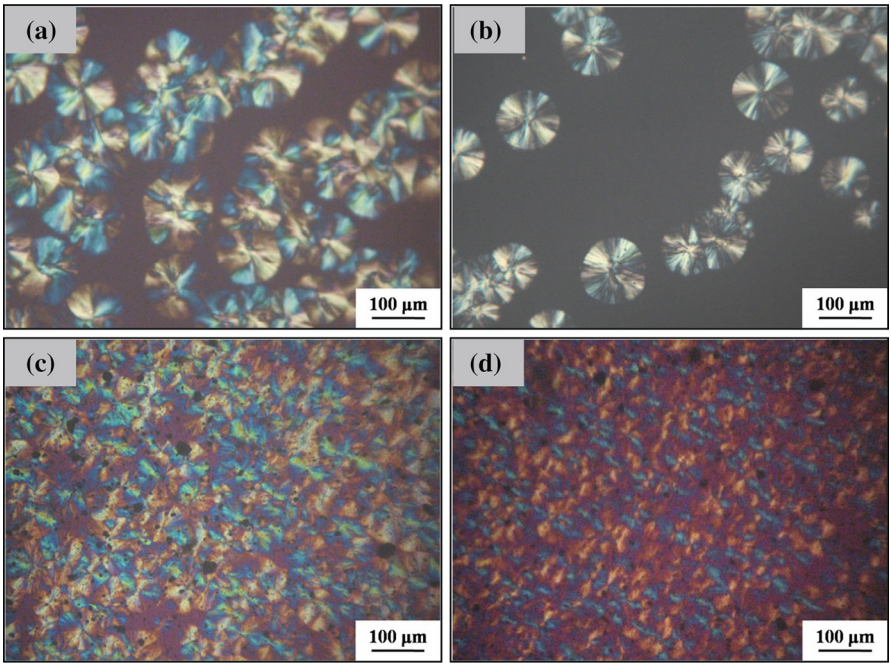

Fig. 2 POM images showing the crystallization morphologies of **a** PLLA, **b** PLLA/PVAc, **c** PLLA/PVAc/CNTs-0.5, **d** PLLA/PVAc/CNTs-1

average diameter of PLLA spherulites is further decreased. This indicates that CNTs accelerate the crystallization of PLLA from the miscible PLLA/PVAc blend. However, it should be stressed that the spherulites morphology of PLLA in the PLLA/PVAc/CNTs-1 sample is still observed, although the interface between spherulites is not clear and the spherulites do not show the integrated spherical shape. This is apparently different from the observations obtained in our previous work, in which only addition of 0.5 wt% CNTs into PLLA matrix accelerated the crystallization of PLLA dramatically and very small spherulites with homogeneous distribution were achieved [22]. Obviously, the presence of PVAc still prevents the nucleation and growth of PLLA spherulites from the miscible PLLA/PVAc blend even if the content of CNTs is increased up to 1 wt%.

To further investigate the different effects of CNTs and PVAc for the crystallization of PLLA, the non-isothermal crystallization behavior of PLLA in different samples was investigated using DSC and the results are shown in Fig. 3. From Fig. 3a, one can see that at cooling rate of 5 °C/min, all the samples show the smooth curves without any exothermic phenomenon induced by the occurrence of crystallization. In other words, PLLA can not crystallize in this condition due to that the relatively high cooling rate which endows the sample less time to crystallize. Figure 3b shows the DSC heating curves of PLLA in different samples and the corresponding thermal parameters are shown in Table 1. For the pure PLLA, one can observe three transitions in the DSC heating curve, attributing to the glass

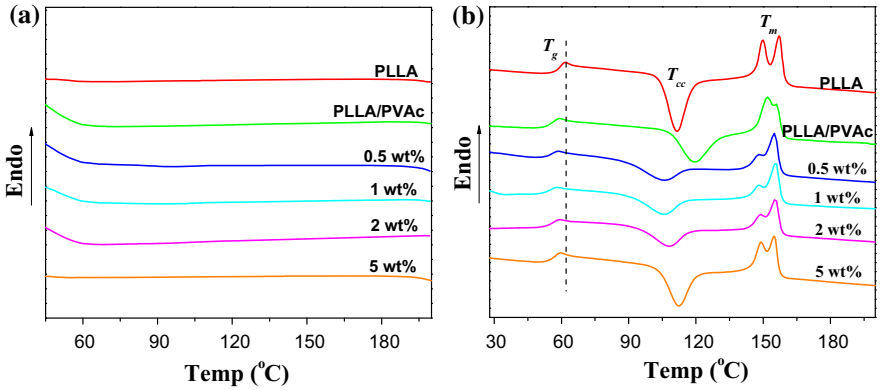

Fig. 3 DSC cooling (**a**) and corresponding heating (**b**) curves showing the crystallization and melting behaviors of representative samples as shown in the *graphs*

Table 1 Thermal properties of different samples obtained from DSC heating scan

Sample	T_g (°C)	T_{cc}	T_m (°C)	ΔH_m (J/g)	ΔH_{cc} (J/g)	X_c (%)
PLLA	59.8	111.4	149.8/157.1	28.22	32.56	0
PLLA/PVAc	56.2	119.6	151.9/155.9	21.36	23.80	0
PLLA/PVAc/CNTs-0.5	56.2	105.3	148.2/155.1	20.77	17.47	4.46
PLLA/PVAc/CNTs-1	56.2	105.4	148.3/155.7	19.78	15.85	5.34
PLLA/PVAc/CNTs-2	56.5	107.8	148.9/155.6	19.83	15.89	5.40
PLLA/PVAc/CNTs-5	57.1	112.3	149.0/154.9	25.11	23.53	2.23

Samples were first cooled from 200 to 0 °C at a cooling rate of 5 °C/min

transition (T_g) at temperature of 59.8 °C, the cold crystallization (T_{cc}) at temperature of 111.4 °C, and the fusion (T_m) of crystalline structure at temperature of 150–157 °C, respectively. Because the pure PLLA does not show apparent crystallization phenomenon during the DSC cooling process, it is suggested that the crystalline structure detected at 150–157 °C is mainly originated from the cold crystallization process occurred at 111.4 °C during the DSC heating process. The double endothermic peaks can be attributed to the melt–recrystallization–melt behaviors of raw crystallites during the DSC heating process. For the blank PLLA/PVAc sample, the T_g of PLLA is decreased to 56.2 °C while the T_{cc} is enhanced up to 119.6 °C. The slight decrease of T_g of PLLA is mainly attributed to the role of PVAc chain segments with smaller T_g (42.4 °C, the corresponding DSC curve is not shown here) which promotes the mobility of PLLA. Generally, the enhanced chain segments mobility of PLLA facilitates the occurrence of cold crystallization during the DSC heating process, resulting in the decrease of T_{cc} as reported in the plasticized PLLA sample [28, 29]. Here, the T_{cc} of the blank PLLA/PVAc sample is enhanced, which is mainly attributed to the molecular chain of PVAc with high

molecular weight preventing the nucleation and growth of PLLA crystallites. Only at relatively high temperature, the chain segments of PLLA have enough energy to exclude the restriction effect of PVAc chain segments. The presence of CNTs does not influence the chain segments of PLLA apparently; therefore, all the composites exhibit the similar T_g to that of the blank PLLA/PVAc blend. However, CNTs induce apparent change of cold crystallization of the PLLA/PVAc/CNTs composites and the crystallization behavior is dependent upon the content of CNTs in the composites. At relatively low CNTs content (0.5 and 1.0 wt%), the T_{cc} of PLLA is decreased to 105 °C, much smaller than that of the blank PLLA/PVAc blend and even smaller than that of pure PLLA, indicating the great nucleation effect of CNTs for the cold crystallization of PLLA during the DSC heating process. Further increasing the content of CNTs induces the slight increase of T_{cc}. For example, the T_{cc} of PLLA/PVAc/CNTs-5 is 112.3 °C, about 7 °C higher than that of PLLA/PVAc/CNTs-1. This can be attributed to the presence of large amounts of CNTs, which preventing the growth of spherulites as reported in the literatures. Similarly, double endothermic peaks are observed for all the composites, suggesting the formation of a large number of crystallites with less perfect structure during the cold crystallization process, which subsequently melt at relatively low temperature and transform into perfect crystalline structure through recrystallization process, the latter crystallites then melt at relatively high temperature. Furthermore, although the previous DSC cooling curves do not show the apparent crystallization of PLLA, from Table 1 one can see that the presence of high content of CNTs really facilitates the crystallization of PLLA, leading to the increase of crystallinity. It should be noted that with further increasing the loading of CNTs above 5 wt%, the network or aggregates of CNTs may be formed [30]. On one hand, the nucleation effect of CNTs may be suppressed due to the aggregation of CNTs; on the other hand, the chain diffusion can be hindered by the CNTs network and crystallization becomes more difficult. Therefore, the resultant crystallization and melting behaviors of composites with high loading of CNTs depend on the competition of effects of nucleation and chain diffusion suppression induced by CNTs.

Effect of annealing treatment on cold crystallization of PLLA

To further understand the crystallization behavior of PLLA in the ternary composites, the amorphous sample was further annealed at 80 °C for 30 min. Figure 4 shows the DSC heating curves of annealed samples and the corresponding thermal properties are shown in Table 2. Pure PLLA still shows the three transitions including glass transition (T_g), cold crystallization (T_{cc}) and melting (T_m) of crystallites. Compared with the thermal properties of unannealed PLLA sample, annealed PLLA exhibits smaller T_{cc}, which can be attributed to the crystallites formed during the annealing process promoting the occurrence of cold crystallization during the DSC heating process. Furthermore, annealed PLLA sample exhibits a single endothermic peak, suggesting that the annealed sample has more perfect crystallites. For the annealed PLLA/PVAc sample, the T_g and T_{cc} are only 54.2 and 108.1 °C, respectively, smaller than the 56.2 and 119.6 °C of the unannealed

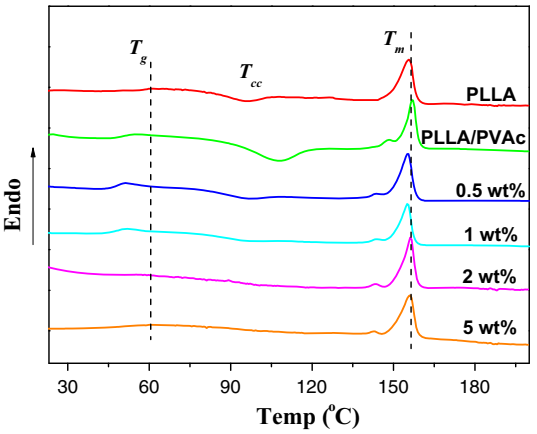

Fig. 4 DSC heating curves of annealed representative samples as showing in the *graph*

Table 2 Thermal properties of annealed samples obtained from DSC heating scan

Sample	T_g (°C)	T_{cc}	T_m (°C)	ΔH_m (J/g)	ΔH_{cc} (J/g)	X_c (%)
PLLA	59.2	95.4	155.7	19.04	4.20	15.96
PLLA/PVAc	50.6	108.1	156.9	20.63	10.93	13.04
PLLA/PVAc/CNTs-0.5	50.8	98.7	156.5	21.05	0.71	27.48
PLLA/PVAc/CNTs-1	48.6	95.9	155.3	21.59	4.32	23.44
PLLA/PVAc/CNTs-2	48.1	95.5	155.2	17.82	2.36	21.20
PLLA/PVAc/CNTs-5	48.1	–	156.0	18.74	–	26.45

Samples were first annealed at 80 °C for 30 min

sample, respectively. As is well known, the T_g is related to the relaxation of chain segments in the amorphous region. During the annealing process, PLLA component in the miscible PLLA/PVAc blend crystallizes, forming the crystalline region with dense chain segments packing. Accordingly, the density of chain segments of PVAc in the amorphous region is increased, leading to more apparent effect for the relaxation of chain segments of PLLA in the amorphous region. Consequently, the blend shows smaller T_g. Similarly, the decrease of T_{cc} of the annealed PLLA/PVAc blend is mainly attributed to the crystallites formed during the annealing process promoting the further cold crystallization of PLLA during the DSC heating scan. For all the composites, the T_g is further decreased due to the increased density of PVAc in the amorphous region resulted by the increase of the crystallinity formed during the annealing process. Specifically, one can see that the cold crystallization during the DSC heating scan becomes inconspicuous and disappears completely at relatively high content of CNTs. This means that the crystallization of PLLA is nearly finished during the annealing process and only a few amounts of PLLA can further crystallize during the DSC heating scan. The variation of the crystallinity shown in Table 2 also shows the different crystallization behaviors during the annealing process. Annealed PLLA sample exhibits the X_{c-DSC} of 16.1%, while for the annealed PLLA/PVAc, the X_{c-DSC} is 13.7%, further indicating that the presence

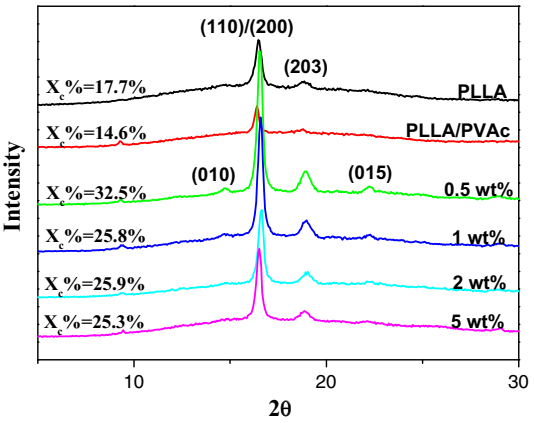

Fig. 5 WAXD spectra of annealed representative samples as shown in the *graph*

of PVAc restricts the cold crystallization of PLLA. For all the composites, the X_{c-DSC} is largely enhanced, proving the nucleation effect of CNTs for the cold crystallization of PLLA.

The crystalline structures of the annealed samples were further detected using WAXD and the results are shown in Fig. 5. For the annealed PLLA, it exhibits the characteristic diffraction peaks at $2\theta = 16.5°$ and 18.9°, attributing to the diffractions of (110)/(200) and (203) crystal planes of α-form of PLLA, indicating the occurrence of cold crystallization of PLLA during the annealing process. For the annealed PLLA/PVAc blend, the intensity of the characteristic diffraction peaks is decreased. However, for all the composites, largely intensified characteristic diffraction peaks are observed, indicating the presence of the improved crystalline structure in the composites. Specifically, for the annealed PLLA/PVAc/CNTs samples containing fewer CNTs, besides the characteristic diffraction peaks of (110)/(200) and (203) crystal planes, one also can see the characteristic diffraction peaks at $2\theta = 14.7°$ and 22.3°, attributing to the diffractions of (010) and (015) crystal planes. The X_{c-WAXD} was calculated and the results are also shown in Fig. 5. The annealed PLLA sample exhibits X_{c-WAXD} of 17.7%. Slightly decreased X_{c-WAXD} (14.6%) is obtained for annealed PLLA/PVAc blend. However, largely increased X_{c-WAXD} is observed for all the composites and the X_{c-WAXD} decreases with increasing content of CNTs. This indicates that a few amounts of CNTs promote the cold crystallization of PLLA from the miscible PLLA/PVAc blend, while the growth of spherulites is restricted at high content of CNTs. Obviously; the observations obtained from WAXD measurement are consistent with those obtained from DSC measurement.

Further understanding about the nucleation of the CNTs in the ternary composites

Different from the dispersion of CNTs in the PLLA matrix, in which the surface of CNTs is completely coated by the chain segments of PLLA, when the CNTs are dispersed in the miscible PLLA/PVAc blend, the molecular absorption on the

surface of CNTs is dependent on the interfacial affinity between CNTs and the two components of the blend. Generally, CNTs can be easily coated by the molecule which has high interfacial affinity to them. The interfacial affinity between CNTs and the polymer component can be evaluated by the calculation of the interfacial tension according to the following equations [31].

Harmonic-mean equation:

$$\gamma_{12} = \gamma_1 + \gamma_2 - 4\left(\frac{\gamma_1^d \gamma_2^d}{\gamma_1^d + \gamma_2^d} + \frac{\gamma_1^p \gamma_2^p}{\gamma_1^p + \gamma_2^p}\right), \tag{3}$$

and geometric-mean equation:

$$\gamma_{12} = \gamma_1 + \gamma_2 - 2\left(\sqrt{\gamma_1^d \gamma_2^d} + \sqrt{\gamma_1^p \gamma_2^p}\right), \tag{4}$$

where γ_i is the surface energy of component i, γ_i^d, and γ_i^p are the dispersive and polar parts of the surface energy of component i, respectively. For the functionalized CNTs with relatively higher polarity, the γ, γ^d and γ^p are 45.3, 18.4 and 26.9 mJ/m^2, respectively, which can be cited from the literature [32]. For the corresponding data of PLLA and PVAc, the surface energy was calculated according to the following equations [33, 34]:

$$\gamma = \gamma^d + \gamma^p, \tag{5}$$

$$\gamma_l(1 + \cos\theta) = 2(\gamma_s^d \gamma_l^d)^{1/2} + 2(\gamma_s^p \gamma_l^p)^{1/2}, \tag{6}$$

where θ is the contact angle; γ_s and γ_l are the surface energy of solid and liquid, respectively; γ_s^d and γ_s^p are the dispersive and the polar components of solid, and γ_l^d and γ_l^p are the dispersive and the polar components of liquid, respectively. To calculate the surface tension, one must know the corresponding surface tension of H_2O and CH_2I_2. These data can be obtained from the literature [35] and the parameters are $\gamma^p = 50.8$ mJ/m^2 and $\gamma^d = 22.5$ mJ/m^2 for H_2O, and $\gamma^p = 2.3$ mJ/m^2 and $\gamma^d = 48.5$ mJ/m^2 for CH_2I_2. In this work, the contact angles of distilled H_2O on the surfaces of PLLA and PVAc films are 74.00 and 57.30, and 43.50 and 67.10 for the CH_2I_2 on the corresponding PLLA and PVAc films, respectively.

As a consequence, the corresponding surface energy data of PLLA and PVAc are shown in Table 3. Accordingly, the interfacial tensions between CNTs and PLLA and between CNTs and PVAc are shown in Table 4. It can be seen that the interfacial tension between PVAc and CNTs is much smaller than that between PLLA and PVAc, indicating that the CNTs have better affinity to the PVAc in

Table 3 Surface energy data of the components

	γ (mJ/m^2)	γ^d (mJ/m^2)	γ^p (mJ/m^2)
PLLA	40.3	32.3	8.0
PVAc	43.6	15.3	28.3
CNTsa	45.3	18.4	26.9

[a] Data were cited from Ref. [32]

Table 4 Interfacial tension as calculated by harmonic-mean and geometric-mean equations

	Based on harmonic-mean equation (mJ/m^2)	Based on geometric-mean equation (mJ/m^2)
$\gamma_{PLLA-CNTs}$	14.04	7.5
$\gamma_{PVAc-CNTs}$	0.32	0.16

comparison with the PLLA. This means that when CNTs are dispersed in the miscible PLLA/PVAc blend, the surface of CNTs is easily coated by PVAc rather than by PLLA. Obviously, the nucleation efficiency of CNTs for the crystallization of PLLA is decreased, leading to relatively smaller nucleation density of PLLA in the PLLA/PVAc/CNTs composite as compared with the present of CNTs in PLLA/CNTs composites [22]. However, it should be noticed that CNTs have large aspect ratio and the large amounts of PLLA in the composites, partial chain segments of CNTs, which is not coated by PVAc, still show the nucleation effect for the crystallization of PLLA, but the growth of PLLA spherulites is restricted by the adjacent chain segments of PVAc. Further work needs to be done to prove the hierarchy distribution of PVAc or PLLA surrounding the CNTs.

Conclusions

In summary, the crystallization behavior of PLLA from the miscible PLLA/PVAc blend induced by CNTs has been comparatively investigated. The results show that PVAc restricts the crystallization of PLLA greatly. CNTs exhibit apparent nucleation effect for the crystallization of PLLA in all conditions including melt crystallization and cold crystallization, leading to the increase of the nucleation density; however, the spherulites growth is still influenced by the PVAc. Further results show that the decreased nucleation efficiency of CNTs in the PLLA/PVAc/CNTs composites in comparison with that in the binary PLLA/CNTs composites is mainly attributed to the better interfacial affinity between CNTs and PVAc, which possibly leads to more PVAc molecule rather than the PLLA molecule around the surface of CNTs and prevents the nucleation and growth of PLLA crystallites on the surface of CNTs.

Acknowledgements Authors express their sincere thanks to the National Natural Science Foundation of China (51473137) for financial support.

References

1. Aruas R, Harte B, Selke S (2004) An overview of polylactides as packing materials. Macromol Biosci 4:835–864
2. Zhang M, Thomas NL (2011) Blending polylactic acid with polyhydroxybutyrate: the effect on thermal, mechanical, and biodegradation properties. Adv Polym Technol 30:67–79
3. Ikada Y, Tsuji H (2000) Biodegradable polyesters for medical and ecological applications. Macromol Rapid Commun 21:117–132

4. Sakai F, Nishikawa K, Inoue Y, Yazawa K (2009) Nucleation enhancement effect in poly(L-lactide) (PLLA)/poly(ε-caprolactone) (PCL) blend induced by locally activated chain mobility resulting from limited miscibility. Macromolecules 42:8335–8342
5. Nijenhuis AJ, Colstee E, Grijpma DW, Pennings AJ (1996) High molecular weight poly(L-lactide) and poly(ethylene oxide) blends: thermal characterization and physical properties. Polymer 37:5849–5857
6. Anderson KS, Lim SH, Hillmyer MA (2003) Toughening of polylactide by melt blending with linear low-density polyethylene. J Appl Polym Sci 89:3757–3768
7. Yokohara T, Yamaguchi M (2008) Structure and properties for biomass-based polyester blends of PLA and PBS. Eur Polym J 44:677–685
8. Tsuji H, Ikada Y (1995) Properties and morphologies of poly(L-lactide) 1.annealing condition effects on properties and morphologies of poly(L-lactide). Polymer 36:2709–2716
9. Ishida S, Nagasaki R, Chino K, Dong T, Inoue Y (2009) Toughening of poly(L-lactide) by blending with rubbers. J Appl Polym Sci 113:558–566
10. Afrifah KA, Matuana LM (2010) Impact modification of polylactide with a biodegradable ethylene/acrylate copolymer. Macromol Mater Eng 295:802–811
11. Hashima K, Nishitsuji S, Inoue T (2010) Structure-properties of super-tough PLA alloy with excellent heat resistance. Polymer 51:3934–3939
12. Liu HZ, Chen F, Liu B, Estep G, Zhang JW (2010) Super toughened poly(lactic acid) ternary blends by simultaneous dynamic vulcanization and interfacial compatibilization. Macromolecules 43:6058–6066
13. Ma P, Hristova-Bogaerds DG, Goossens JGP, Spoelstra AB, Zhang Y, Lemstra PJ (2012) Toughening of poly(lactic acid) by ethylene-*co*-vinyl acetate copolymer with different vinyl acetate contents. Eur Polym J 48:146–154
14. Fu Y, Liao L, Yang L, Lan Y, Mei L, Liu Y, Hu S (2013) Molecular dynamics and dissipative particle dynamics simulations for prediction of miscibility in polyethylene terephthalate/polylactide blends. Mol Simul 39:415–422
15. Lee JB, Lee YK, Choi GD, Na SW, Park TS, Kim WN (2011) Compatibilizing effects for improving mechanical properties of biodegradable poly (lactic acid) and polycarbonate blends. Polym Degrad Stab 96:553–560
16. Tsuji H, Sawada M, Bouapao L (2009) Biodegradable polyesters as crystallization-accelerating agents of poly(L-lactide). ACS Appl Mater Inter 1:1719–1730
17. Gajria AM, Davé V, Gross RA, McCarthy SP (1996) Miscibility and biodegradability of blends of poly(lactic acid) and poly(vinyl acetate). Polymer 37:437–444
18. Li Y, You J (2011) Micro-phase separation and crystallization behavior of amorphous oriented PLLA/PVAc blends during heat treatment under strain. Polymer 52:2964–2969
19. Zhang GB, Zhang JM, Wang SG, Shen DY (2003) Miscibility and phase structure of binary blends of polylactide and poly(methyl methacrylate). J Polym Sci Part B Polym Phys 41:23–30
20. Shirahase T, Komatsu Y, Tominaga Y, Asai S, Sumita M (2006) Miscibility and hydrolytic degradation in alkaline solution of poly(L-lactide) and poly(methyl methacrylate) blends. Polymer 47:4839–4844
21. Shirahase T, Komatsu Y, Marubayashi H, Tominaga Y, Asai S, Sumita M (2007) Miscibility and hydrolytic degradation in alkaline solution of poly(L-lactide) and poly(*p*-vinyl phenol) blends. Polym Degrad Stab 92:1626–1631
22. Li YL, Wang Y, Han L, Xiang FM, Zhou ZW (2009) Crystallization improvement of poly(L-lactide) induced by functionalized multiwalled carbon nanotubes. J Polym Sci Part B Polym Phys 47:326–339
23. Xu ZH, Niu YH, Wang ZG, Li H, Yang L, Qiu J, Wang H (2011) Enhanced nucleation rate of polylactide in composites assisted by surface acid oxidized carbon nanotubes of different aspect ratios. ACS Appl Mater Interfaces 3:3744–3753
24. Xu JZ, Chen T, Yang CL, Li ZM, Mao YM, Zeng BQ, Hsiao BS (2010) Isothermal crystallization of poly(L-lactide) induced by graphene nanosheets and carbon nanotubes: a comparative study. Macromolecules 43:5000–5008
25. Tao F, Nysten B, Baudouin AC, Thomassin JM, Vuluga D, Detrembleur C, Bailly C (2011) Influence of nanoparticle–polymer interactions on the apparent migration behaviour of carbon nanotubes in an immiscible polymer blend. Polymer 52:4798–4805
26. Gao Y, Wang Y, Shi J, Bai HW, Song B (2008) Functionalized multi-walled carbon nanotubes improve nonisothermal crystallization of poly(ethylene terephthalate). Polym Test 27:179–188

27. Fischer EW, Sterzel HJ, Wegber G (1973) Investigation of the structure of solution grown crystals of lactide copolymers by chemical reactions. Kolloid ZZ Polym 251:980–990
28. Kulinski Z, Piorkowska E (2005) Crystallization, structure and properties of plasticized poly(L-lactide). Polymer 46:10290–10300
29. Li YL, Wu HY, Wang Y, Liu L, Han L, Wu J, Xiang FM (2010) Synergistic effects of PEG and MWCNTs on crystallization behavior of PLLA. J Polym Sci Part B Polym Phys 48:520–528
30. Wu DF, Wu L, Zhou WD, Sun YR, Zhang M (2010) Relations between the aspect ratio of carbon nanotubes and the formation of percolation networks in biodegradable polylactide/carbon nanotube composites. J Polym Sci Part B Polym Phys 48:479–489
31. Wu S (1982) Polymer interface and adhesion. Marcel Dekker Inc., New York
32. Nuriel S, Liu L, Barber AH, Wagner HD (2005) Direct measurement of multiwall nanotube surface tension. Chem Phys Lett 404:263–266
33. Fowkes FM (1962) Determination of interfacial tensions, contact angles, and dispersion forces in surfaces by assuming additivity of intermolecular interactions in surfaces. J Phys Chem 66:382–389
34. Owens DK, Wendt RC (1969) Estimation of the surface free energy of polymers. J Appl Polym Sci 13:1741–1747
35. Dalai EN (1987) Calculation of solid surface tensions. Langmuir 3:1009–1015